

Construction of Continuous Magnetic Cooling Apparatus with Zinc Soldered PrNi₅ Nuclear Stages

S. Takimoto · R. Toda · S. Murakawa · Hiroshi Fukuyama

Received: date / Accepted: date

Abstract We report design details of the whole assembly of a compact and continuous nuclear demagnetization refrigerator (CNDR) with two PrNi₅ nuclear stages, which can keep temperature below 1 mK continuously, and test results of a new thermal contact method for the PrNi₅ stage using Zn soldering rather than Cd soldering. By measuring a residual electrical resistance of a short test piece, the thermal contact resistivity between the PrNi₅ rod and an Ag wires thermal link was estimated as $1.8 \pm 0.1 \times 10^{-4} T^{-1} \text{ Km}^2 \text{ W}^{-1}$. Based on this value and 2D numerical and 1D analytical thermal simulations, the largest possible temperature gradient throughout the nuclear stage was calculated to be negligibly small ($\leq 2\%$) at 1 mK under a 10 nW heat leak, the expected cooling power of the CNDR.

Keywords nuclear demagnetization refrigerator · PrNi₅ · contact resistance

1 Introduction

Recently, a sub-mK temperature environment is recognized as one of the frontiers in research fields of material science [1], nanoelectronics [2], and cryogenic particle detector [3]. The nuclear demagnetization refrigerator (NDR) with copper nuclear stage is a standard equipment to achieve such extremely low temperatures [4]. However, construction and operation of NDRs are technically demanding, which has been preventing non-experts

from making use of the sub-mK environment. In order to overcome the limitations, we recently proposed the concept of continuous refrigeration using two PrNi₅ nuclear demagnetization stages and a dilution refrigerator connected in series each other via two superconducting heat switches [5]. The numerical simulations under realistic conditions showed that this new type of refrigerator, the continuous nuclear demagnetization refrigerator (CNDR), can keep the sample temperature at 0.8 mK with a cooling power of 10 nW [5]. Developments of CNDR are now actively conducted [6,7,8].

In this article, after showing an updated total design of our CNDR in Sec. 2, we report construction details of the PrNi₅ nuclear stage, one of major parts of the CNDR (Sec. 3). We tested a new soldering method with Zn for PrNi₅ and estimated a thermal contact resistivity of the Zn contact between a PrNi₅ rod and Ag wires from electrical resistance measurements (Sec. 4). Then, using known resistivities of all parts, a possible temperature gradient through the PrNi₅ nuclear stage was evaluated from numerical and analytical calculations on thermal models (Sec. 5).

2 Practical Design of the CNDR

Figure 1 shows a schematic diagram of our CNDR. The CNDR consists of four major parts, (1) a standard dilution refrigerator which has a cooling power of at least 100 μW at 100 mK, (2) two PrNi₅ nuclear stages, (3) two shielded superconducting (SSC) magnets [7] and (4) two superconducting Zn heat switches. The PrNi₅ stages are connected in series between the sample stage and the mixing chamber of the dilution refrigerator through the two heat switches. The CNDR can keep temperature below 1 mK continuously with a cooling

S. Takimoto
E-mail: takimoto@crc.u-tokyo.ac.jp

H. Fukuyama
E-mail: hiroshi@kelvin.phys.s.u-tokyo.ac.jp

Cryogenic Research Center, The University of Tokyo, 2-11-16
Yayoi, Bunkyo-ku, Tokyo, Japan

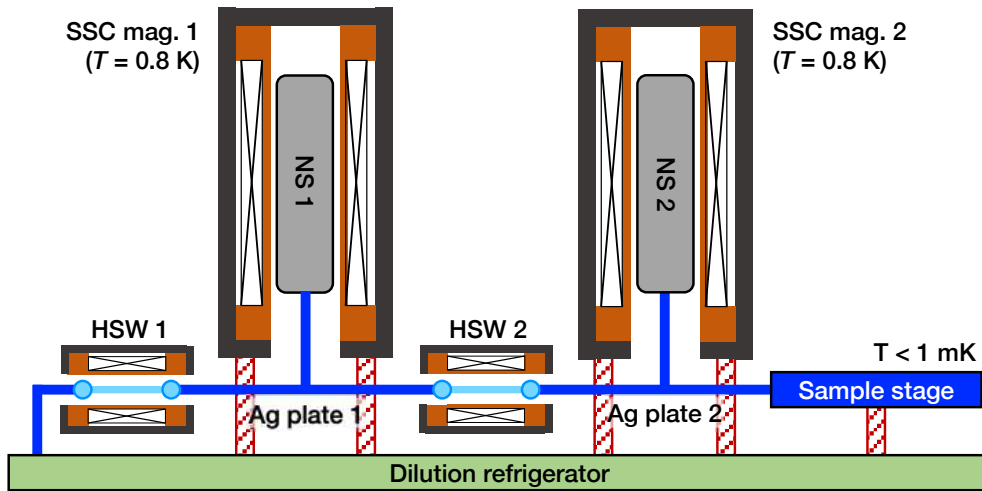


Fig. 1 Schematic figure of the CNDR. The two PrNi_5 nuclear stages with the two SSC magnets (SSC mag.1, 2) are connected in series through the two superconducting heat switches (HSW1, 2). All magnets are thermally anchored to the still of dilution refrigerator.

power of 10 nW if the total thermal resistance among the four components is less than the value corresponding to a few hundreds $\text{n}\Omega$ in the electrical resistance unit [5].

Figure 2 shows a three-dimensional CAD image of our latest version of CNDR. The nuclear stages and other components are assembled on a Cu base plate which is connected directly to the mixing chamber. The two SSC magnets are thermally anchored to the still of the dilution refrigerator and mechanically supported by Vespel SP-22 thermal insulation rods from the base plate. Three of four Ag thermal links for the heat switches and six Ag thermal links for the nuclear stages are tightly connected to two Ag plates of 5 mm thick with M4 $\text{Si}_{0.15}\text{Ag}_{0.85}$ (Tokuriki Honten Co., Ltd.) screws so as to be demountable. The cross section of each Ag thermal link is $9 \times 5 \text{ mm}^2$. The contact areas of these parts are gold-plated of 3–4 μm thickness to reduce the contact thermal resistance [9]. The maximum dimensions of the whole assembly of this CNDR are 160 mm in length, 84 mm in width and 240 mm in height, which are compact enough to be installable in most of dilution refrigerators.

3 Zinc Soldering of PrNi_5 Nuclear Stage

It is important to achieve a better thermal contact between a nuclear coolant and a thermal link to minimize a temperature gradient between them under finite heat flows. Figure 3 (a) shows a cross section of the PrNi_5 nuclear stage of the CNDR. Each stage consisting of three PrNi_5 rods of about 6 mm diameter and 120 mm long is soldered to the thermal link made of 15 Ag wires

of 1 mm diameter with Zn as described in more detail later. It is noted that we cannot apply common press contact here because PrNi_5 is so brittle and can easily crack under stress. The other ends of the Ag wires are electron-beam (EB) welded to the silver block (see Fig. 3 (b)). The depth and lateral dimensions of the welded part are 6 mm and $8 \times 6 \text{ mm}^2$, respectively. After the EB welding, the assembled Ag thermal link was annealed at 800°C for 3 hours in an O_2 flow ($P \sim 0.1 \text{ Pa}$). The residual resistivity ratio (RRR) of the Ag wire was increased from 300 to 2,300 by this heat treatment. From the four-wire measurement at 4.2 K, we determined a residual electrical resistance of the EB welded part to be $13.5 \pm 1.0 \text{ n}\Omega$. This is lower than resistances of other parts throughout the nuclear stage (see later discussions). RRR of the PrNi_5 rod is 42.

There are three common soldering agents to attach the PrNi_5 rod to the thermal link, that are Cd [10, 11, 12, 13], In [14] and Sn [15]. Cd has most commonly been used in the previous works because of its low superconducting critical field ($H_c = 3.0 \text{ mT}$). Note that H_c limits the final field of demagnetization cooling. However, the problem of Cd is that it is toxic. In has a ten times higher H_c than that of Cd and is mechanically rather weak. Sn has also a high H_c , and sometimes the cold brittleness due to structural transformation [16] causes trouble. In this work, as a substitute soldering agent for Cd, we tested to use Zn which has a low enough H_c ($= 5.3 \text{ mT}$) and low health damage. A drawback of Zn is a little higher melting temperature (420°C) (see Table 1).

We evaluated the performance of the Zn soldering for the PrNi_5 rod and Ag wires by making a short test piece shown in Fig. 4(a). Figure 4(b) shows a home-

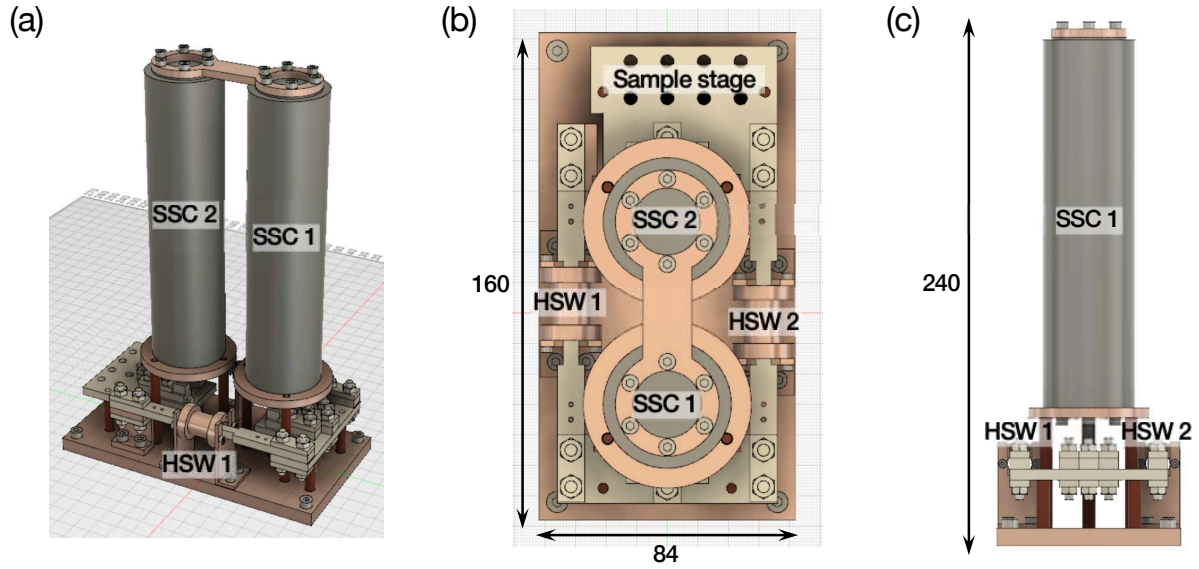


Fig. 2 Three-dimensional CAD model of the CNDR. (a) whole view, (b) top view, and (c) side view of the CNDR. The unit of the dimensions denoted is millimeter.

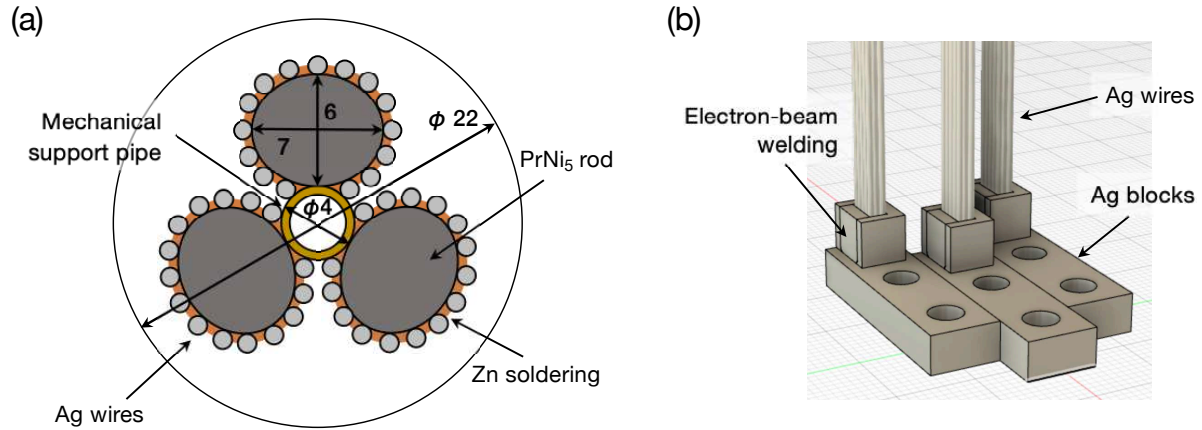


Fig. 3 (a) Cross section of the PrNi_5 nuclear stage. The bore diameter of the SSC magnet is 22 mm. (b) Far end of the nuclear stage. The Ag blocks e-beam welded with the Ag wires are attached to the Ag plate with silicon-silver screws.

Table 1 Various soldering agents for the PrNi_5/Ag contact.

	Melting temp. T_m ($^{\circ}\text{C}$)	Supercond. T_c (K)	Supercond. H_c (mT)	Flux	Note
Cd	321	0.56	3.0	ZnCl_2 or NH_4Cl	toxic
In	157	3.40	29.3		high H_c , soft
Sn	232	3.75	30.9		high H_c , brittle
Zn	420	0.85	5.3	$\text{ZnCl}_2 + \text{NH}_4\text{Cl}$	high T_m

made furnace used in this test where a heater wire is wound around a high-purity (99.6 %) alumina furnace tube of 24 mm in inner diameter and 500 mm in height with a closed bottom. The alumina tube, in which molten Zn is filled, are thermally insulated by a rock wool. The tube temperature was kept around 480 $^{\circ}\text{C}$ with a PID controller during the soldering. The

test piece was first immersed in a 10 wt% water solution of NaOH kept at 80 $^{\circ}\text{C}$ for 5 minutes for degreasing. After washing it with water, it was immersed in a 10 wt% water solution of HCl kept at 30 $^{\circ}\text{C}$ for 5 minutes for removing surface oxides. After washing it with water, it was then immersed in a flux, a 25 wt% water solution of a mixture of ZnCl_2 (56 wt%) and NH_4Cl (44 wt%),

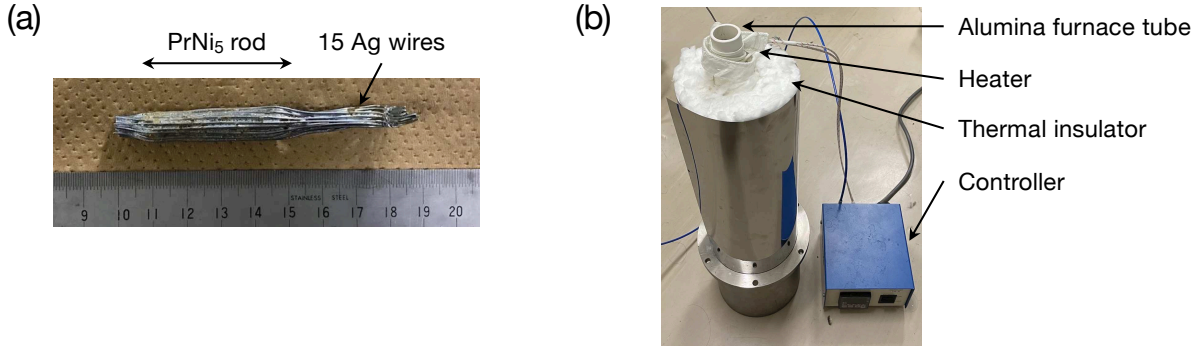


Fig. 4 (a) Short test piece for Zn soldering of the PrNi₅/Ag contact. (b) Home-made furnace used for the Zn soldering.

kept at 60 °C, and finally dipped in the molten Zn for 2 minutes for soldering.

4 Measurement of the Zn Soldered PrNi₅/Ag Contact Resistance

The thermal contact resistivity of the Zn-soldered Ag and PrNi₅ contact was evaluated from a measurement of the total resistance of the test piece in the configuration shown in Fig. 5(a). The red and blue pieces here correspond to the Ag wires (A) and the PrNi₅ rod (B), respectively. The contact area between A and B is denoted as C. The total resistance R_{tot} of this configuration is analytically given as the following equation [17] based on the ladder model shown in Fig. 5(b):

$$R_{\text{tot}} = \frac{r_A r_B}{r_A + r_B} l + \frac{r_A^2 + r_B^2}{r_A + r_B} l_0 \coth\left(\frac{l}{l_0}\right) + \frac{2r_A r_B}{r_A + r_B} l_0 \left[\sinh\left(\frac{l}{l_0}\right)\right]^{-1}, \quad (1)$$

where

$$r_A = \frac{\rho_A}{w_A d_A}, \quad r_B = \frac{\rho_B}{w_B d_B}, \quad \text{and} \quad l_0 = \sqrt{\frac{\rho_C}{(r_A + r_B) w_C}}. \quad (2)$$

Here, ρ_A and ρ_B are volume resistivities of A and B, respectively, and ρ_C is a contact resistivity. l and w are the length and the width of the contact area, respectively, and d is the thickness of each piece. Since the ladder model is applicable to both thermal (t) and electrical (e) flow problems, superscripts t or e will be put on variables when we want to specify either t- or e-resistance in the following.

We measured R_{tot}^e of the test piece at 4.2 K in liquid ⁴He by using the four-terminal method shown in Fig. 5(c). ρ_A^e and ρ_B^e were determined from independent measurements for each Ag and PrNi₅ pieces at 4.2 K. By substituting these values to eq.(1), we have $\rho_C^e =$

$4.3 \pm 0.2 \text{ p}\Omega\text{m}^2$. Since conduction electrons are carriers of both electrical and thermal flows in pure metals and metallic compounds at millikelvin temperatures, one can convert ρ^e to ρ^t assuming the Wiedemann-Franz law with the Lorenz number $L (= 2.45 \times 10^{-8} \text{ W}\Omega\text{K}^{-2})$. The fairly good applicability of this law to PrNi₅ is verified down to 100 mK [18]. Then, we have the thermal contact resistivity as $\rho_C^t = (1.8 \pm 0.1) \times 10^{-4} T^{-1} \text{ Km}^2\text{W}^{-1}$.

The obtained electrical resistivity ρ_C^e of the Zn soldered PrNi₅/Ag contact, which gives a total contact resistance of 4 nΩ for each PrNi₅ rod, is sufficiently low for our purpose. This can easily be understood if compared with the total electrical resistance of 140 nΩ throughout the whole PrNi₅ stage in Greywall's single-stage nuclear demagnetization refrigerator [12]. In the next section, we will confirm this more quantitatively.

5 Simulations for Temperature Gradient in the Nuclear Stage

Using the ρ_A^t , ρ_B^t and ρ_C^t values obtained in the previous section, one can evaluate a temperature difference $\Delta T (> 0)$ throughout the nuclear stage under a given heat flow. In order to estimate the largest possible ΔT , we made numerical simulations based on the finite element method under a constrain that the temperature (T_0) along the central (z) axis of the PrNi₅ rod is always kept at 1 mK as shown in Fig. 6(a) left. The constrain is equivalent to neglecting cooling powers associated with slow demagnetization of nuclear spins in off-axial segments within the PrNi₅ rod. This intentionally increases a radial (r) temperature gradient than the actual situation. For simplicity, we also applied axisymmetry about the central axis to the model. This means that no azimuthal component of heat flow is considered. A constant heat flow of $\dot{Q} = 3.3 \text{ nW}$, which is one third of the expected total cooling power of our CNDR, was introduced from the top end of the Ag wires (see Fig. 6(a) left). Thus the temperature at that end is $T_0 + \Delta T$.

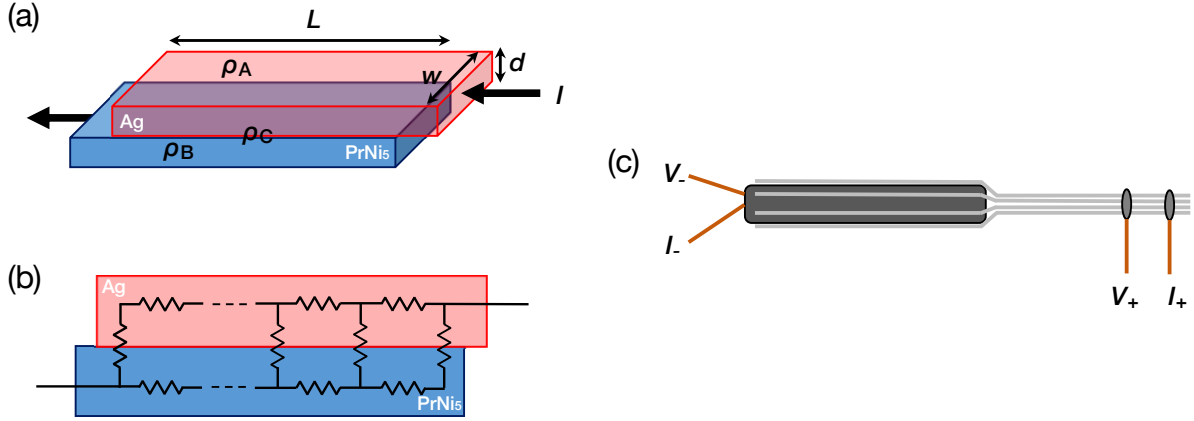


Fig. 5 (a) Schematic configuration for measurement of the thermal contact resistivity between the Ag wires and PrNi₅ rod. (b) Resistor ladder model for the configuration shown in (a). (c) Four-terminal setup for the R_{tot}^e measurement to estimate the contact resistivity in the Zn soldered PrNi₅ nuclear stage.

The simulations were carried out using an open source software (FEMM: Finite Element Method Magnetics by David Meeker). In the simulation, a z - r (two dimensional: 2D) plane of the nuclear stage is divided to 16,000 elements.

Results of the simulation for six different ρ_C^e ($= 4.3, 20, 40, 60, 80, 100 \text{ p}\Omega\text{m}^2$) are shown as the dots in Fig. 6(b). For the ρ_C^e value ($= 4.3 \pm 0.2 \text{ p}\Omega\text{m}^2$) we obtained with the Zn soldering, ΔT is expected to be less than $20 \text{ }\mu\text{K}$ at $T_0 = 1 \text{ mK}$, which is negligibly small. $\Delta T/T_0$ is not sensitive to ρ_C^e and will not exceed 10% unless ρ_C^e becomes larger by two orders of magnitude.

The dashed line in Fig. 6(b) is an expected behavior from the one-dimensional (1D) model considering serially connected three thermal resistances which are the resistance of the Ag wires (R_A^t) above the stage, that of the PrNi₅ (R_B^t) and the contact resistance (R_C^t) between them (see Fig. 6(a) right). R_B^t and R_C^t are calculated from ρ_B^t and ρ_C^t neglecting the resistance of the Ag wires over the length of the PrNi₅ rod and considering only the r component of heat flow. This simplification resembles to the constraint of fixed T_0 ($= 1 \text{ mK}$) along the z axis in the 2D numerical simulation described above. The analytical solution of the 1D model is expressed as:

$$\Delta T = \sqrt{T_0^2 + \frac{\dot{Q}}{\pi L} (A \cdot \rho_A^e + B \cdot \rho_B^e + C \cdot \rho_C^e)} - T_0, \quad (3)$$

where $A(= 4.27 \times 10^4 \text{ m}^{-1})$, $B(= 28.3 \text{ m}^{-1})$, and $C(= 5.85 \times 10^3 \text{ m}^{-2})$ are geometrical factors. As can be seen in Fig. 6(b), the 1D analytical model gives slightly smaller ΔT values than the 2D numerical simulation, because the temperature variation along the z direction is neglected. However, the difference (8–16 %) is small

and the 1D model is much simpler to calculate, so it is a more convenient estimator of ΔT .

6 Conclusion

We described design details of the whole assembly of the continuous nuclear demagnetization refrigerator (CNDR) which is so compact that it can be installed on the mixing chamber of an existing dilution refrigerator. We focused on the design of the PrNi₅ nuclear stage, a central part of the CNDR, in this article. As an alternative to the widely-used Cd soldering thermal contact for PrNi₅, the Zn soldering was proposed and tested. From the residual electrical resistance measurements of a short test piece, the thermal contact resistivity between the PrNi₅ rod and the Ag wires was estimated as $1.8 \pm 0.1 \times 10^{-4} T^{-1} \text{ Km}^2\text{W}^{-1}$ assuming the Wiedemann-Franz law. This is favorably compared with the previously reported contact resistivities for other metals and soldering agents. Using known resistivities of all major parts of the CNDR, we evaluated the largest possible temperature gradient $\Delta T/T$ throughout the nuclear stage from the 2D numerical and 1D analytical calculations. The calculations show a negligibly small $\Delta T/T$ ($\leq 2\%$) at 1 mK under a 10 nW heat leak, which is an expected cooling power of the CNDR. All parts of the CNDR are now being assembled anticipating the first cooling test.

Acknowledgements We thank the machine shop of the School of Science, the University of Tokyo for machining most of the parts of CNDR. ST was supported by Japan Society for the Promotion of Science through Program for Leading Graduate Schools (MERIT).

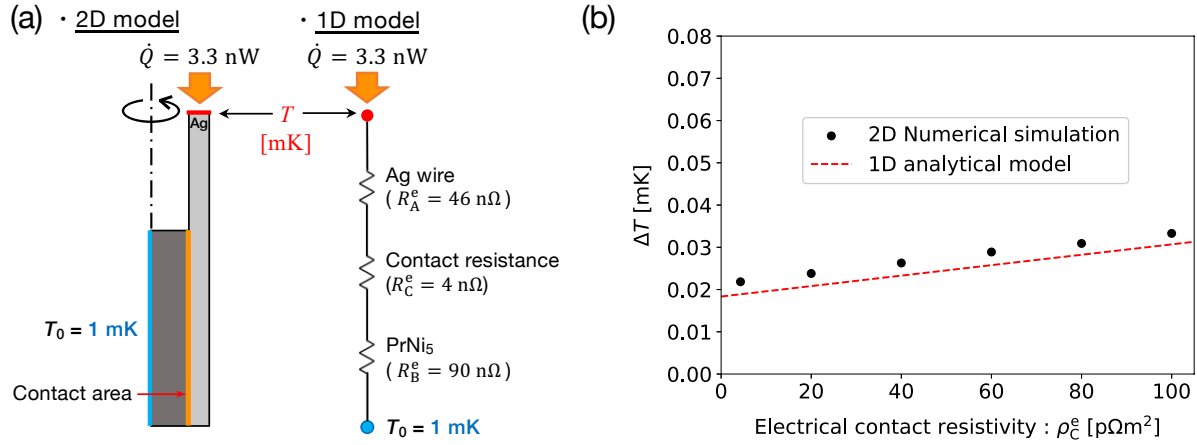


Fig. 6 (a) Two types of thermal models to estimate the largest possible temperature gradient (ΔT) throughout the PrNi₅ nuclear stage. (left) 2D model for numerical simulation by the finite element method. (right) 1D analytical model. (b) ΔT as a function of the Zn-soldering contact resistivity (ρ_C^e) estimated from the 2D (dot) and 1D (dashed line) models.

References

1. A. C. Clark, K. K. Schwarwalder, T. Bandi, D. Maradan, and D. M. Zumbuhl, *Rev. Sci. Instrum.* **81**, 103904 (2010).
2. M. Palma, D. Maradan, L. Casparis, T.-M. Liu, F. N. M. Froning, and D. M. Zumbuhl, *Rev. Sci. Instrum.* **88**, 043902 (2017).
3. P. Shirron, D. Wegel, M. DiPirro, and S. Sheldon, *Nuclear Instruments and Methods in Physics Research A* **559**, 651 (2006).
4. F. Pobell, *Matter and Methods at Low Temperatures*, 3rd ed. (Springer, Berlin, 2007).
5. R. Toda, S. Murakawa, and H. Fukuyama, *J. Phys.: Conf. Ser.* **969**, 012093 (2018).
6. D. Schmoranzer, R. Gazizulin, S. Triqueneaux, E. Collin, A. Fefferman, *J. Low Temp. Phys.* **196**(1-2), 261 (2019).
7. S. Takimoto, R. Toda, S. Murakawa, and H. Fukuyama, *J. Low Temp. Phys.* **201**, 179 (2020).
8. D. Schmoranzer, J. Butterworth, S. Triqueneaux, E. Collin, A. Fefferman, *Cryogenics* **110**, 103119 (2020).
9. T. Okamoto, H. Fukuyama, H. Ishimoto, and S. Ogawa, *Rev. Sci. Instrum.* **61**, 1332 (1990).
10. R. Mueller, C. Buchal, H. Folle, M. Kubota, and F. Pobell, *Cryogenics* **20**(7), 395 (1980).
11. K. Andres and S. Darack, *Physica B+C* **86-88**(PART 3), 1071 (1977).
12. D. Greywall, *Phys. Rev. B* **31**, 2675 (1985).
13. J. Parpia, W. Kirk, P. Kobiela, T. Rhodes, Z. Olejniczak, and G. Parker, *Rev. Sci. Instrum.* **56**, 437 (1985).
14. S. Wieggers, T. Hata, C. Kranenburg, P. van de Haar, R. Jochemsen, and G. Frossati, *Cryogenics* **30**(9), 770 (1990).
15. H. Ishimoto, N. Nishida, T. Furubayashi, M. Shinohara, Y. Takano, Y. Miura, and K. Ono, *J. Low Temp. Phys.* **55**(1-2), 17 (1984).
16. E. Cohen and A. K. W. A. van Lieshout, *Z. Physik. Chem.* **173**, 32 (1935).
17. H. Ishimoto, H. Fukuyama, N. Nishida, Y. Miura, Y. Takano, T. Fukuda, T. Tazaki, and S. Ogawa, *J. Low Temp. Phys.* **77**, 133 (1989).
18. H. C. Meijer, G. J. C. Bots, and H. Postma, *Physica* **107B**, 607 (1981).